Molecular growth of PAH-like systems induced by oxygen species: experimental and theoretical study of the reaction of naphthalene with HO (2Π3/2), O (3P), and O2(3Σ−g)

UNIVERSITÀ DEGLI STUDI DI TORINO

Molecular growth of PAH-like systems induced by oxygen species: experimental and theoretical study of the reaction of naphthalene with HO ($^2\Pi_{3/2}$), O (^{3}P), and O_2 ($^3\Sigma_g^-$).

Marco Scapinello
CNR-IMCB, U.O.S. Trento, via Sommarive 14, I-38123 Povo, Trento, Italy.
Luca Matteo Martini, Paolo Tosi[a]
Dipartimento di Fisica, Università di Trento, Via Sommarive 14, I-38123 Povo, Italy
Andrea Maranzana and Glauco Tonachini[b]
Dipartimento di Chimica, Università di Torino, Corso Massimo D'Azeglio 48, I-10125 Torino, Italy

Abstract. To assess if reactions with oxygen species can induce a mass increase of polycyclic aromatic hydrocarbons, we exposed naphthalene molecules to an oxidative gas flow containing the radicals H and HO ($^2\Pi_{3/2}$) and the diradicals O (^{3}P) and O_2 ($^3\Sigma_g^-$). We observed the formation of 1- and 2-naphtol, 1,4-naphthoquinone, naphthalene-derived cyclic ethers, an ester from ring opening, and ether adducts containing two naphthalene units. We investigated possible reaction pathways as a function of temperature by density functional calculations. We found that the reactivity is characterized by HO, O and H addition to naphthalene, or by H abstraction from it, with roles depending on temperature. In conclusion, oxygen species can promote, under the experiment conditions, mainly naphthalene oxidation and, only to a lesser extent, substantial molecular growth, with an efficiency that the calculations indicate to depend on the system temperature. Future experiments should try to quantify key species to allow defining the relative importance of the various reaction mechanisms uncovered by *ab initio* calculations.

keywords: naphthalene, plasma, oxygen, oxidation products, DFT

Electronic Supplementary Information (ESI) available: See DOI: …

[a] Author to whom correspondence should be addressed: tosi@science.unitn.it
[b] Author to whom correspondence should be addressed: glauco.tonachini@unito.it

Introduction

Understanding the formation, growth, and possible oxidation of polycyclic aromatic hydrocarbons (PAHs, of which naphthalene is the lightest representative) is of interest in different fields, as combustion,[1,2,3,4,5,6] environment[7] and health, and even astrochemistry.[8,9,10,11] Chemical transformations of the hydrocarbon skeleton can see the intervention of small oxidants, among which ground state O and O_2. Oxidation can accompany growth,[12,13,14,15] extending over the entire course of PAH and soot formation, but can also consume and destroy carbonaceous particles, depending on the combustion conditions, in particular at higher temperatures.[16,17,18,19,20,21,22] We feel that the role of oxidation processes in the growth of PAHs needs further clarification.[23,24,25]

A practical way to study PAH oxidation and growth is by plasma techniques. For instance, treating benzene in an air plasma produces phenol, together with biphenyl ($C_{12}H_{10}$) and products with elemental formula $C_6H_6O_2$, $C_{12}H_{10}O$, and $C_{12}H_{10}O_2$.[26] the plasma conversion of naphthalene gives several byproducts, including benzaldehyde, acetophenone, benzoic acid, salicylic acid, phenylethyne, benzoic acid phenyl ester, and 1-hydroxycyclohexyl phenyl ketone (methanone).[27]

To get some insights on the role of oxidative reactions in the growth of polycyclic aromatic hydrocarbons, we chose naphthalene as a model system, mainly because of its high vapor pressure.[5b] Thus, we exposed naphthalene molecules to the outflow of a He/O_2 discharge and detected the reaction products. We observed both oxidation and molecular growth, the latter to a lesser extent. To rationalize the experimental results, we carried out DFT calculations to explore possible reaction pathway to the observed products.[28]

Experimental Method

To investigate the reactivity of oxygen species with naphthalene we have developed an experimental setup (sketched in Figure 1) composed by an atmospheric pressure RF plasma jet to produce atomic oxygen,[29,30] an evaporator to produce gas-phase naphthalene, and a reactor where the reactants mix together.

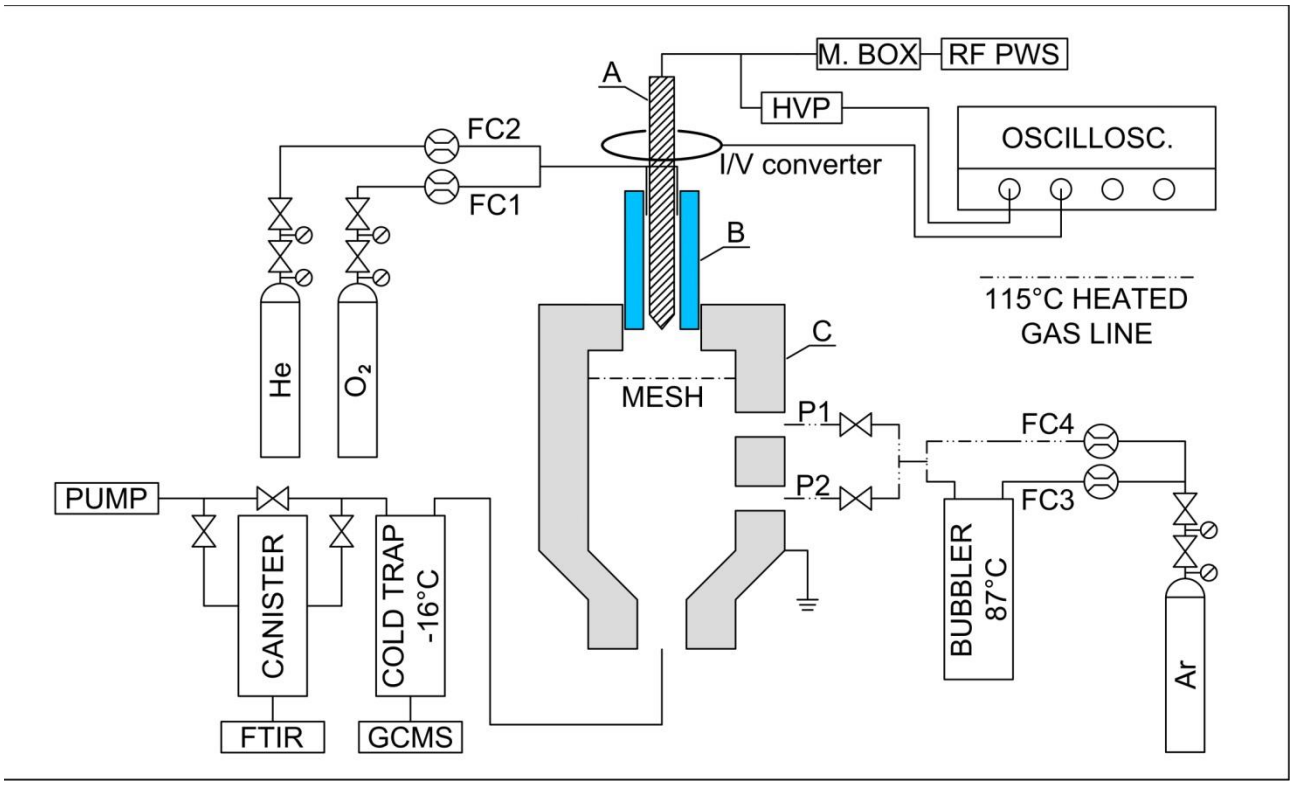

Figure 1. Scheme of experimental setup. RF PWS: RF power supply; M. BOX: matching box; HVP: high voltage probe; FC1, FC2, FC3, FC4: mass flow controllers; A: tungsten electrode; B: quartz tube; C: metallic reactor.

Naphthalene (99,9% purity) was melted in a bubbler at the temperature of 87 ± 1°C, and transported into a heated pipe (115°C) by a gentle flow of argon (500 sccm – FC3). The pipe contains a carrier flow of Argon (1000 sccm – FC4) that transports naphthalene into the reactor C, where the pressure is around the atmospheric value. We estimate the temperature to be about 400 K. Here the final concentration of naphthalene is estimated to be around 4×10^{16} molecules/cm^3. In the reactor the naphthalene flow intercepts the discharge flow at different distances from the counter electrode (P1, 3 mm, and P2, 13 mm). The discharge feed gases, helium and oxygen, are controlled by two mass flow controllers (FC2, FC1). The total flow is set at 2000 sccm, the oxygen concentration can vary between 0 and 4.0%.

In nominal "pure" helium plasma, O_2 (less than 2 ppm) and humidity (less than 10 ppm) were still present in traces, and are responsible for the residual production of oxygen oxidants. In fact, in a similar set up we detected about 10^{12} molecules/cm^3 of HO by LIF measurements.[31]

The discharge is sustained by a power supply (RF5S-RFPP) at 13.56 MHz via a matching box (AM5-RFPP), and occurs between the HV tungsten electrode (A, 1 mm of

diameter, 170 mm of length) and the grounded mesh. To measure the power, voltage and current probes (Tektronix-P6015A and Magnelab CT-01-b, respectively) were connected between the matching box and the tungsten electrode. V/I signals were recorded by a digital oscilloscope (WaveSurfer 104MXs-A, LeCroy, 1GHz). The dissipated power was calculated by integrating the voltage times the current, by taking into account the time delay introduced by the probes. The actual power dissipated into the plasma was calculated as difference between the power values measured with and without gas (discharge on and off, respectively).[32] The plasma power turns out to depend on both the applied voltage and the gas composition. In particular by increasing the O_2 percentage, the plasma power decreases.

At the exit of the reactor, chemicals were condensed in a cold trap, T = -16 ± 1°C. Uncondensed gases were collect in a canister and analyzed by a FT-IR spectrometer (Bruker Equinox 55), with qualitative detection of CO_2 and CO in traces.

Condensed products were dissolved in 5 ml of acetonitrile and semi-quantitatively analyzed by chromatographic techniques, by using a Finningam Trace GC Ultra with both MS and FID detector. A DB-5 column (30 m length × 0.25 mm od × 0.25 µm width) was used. The carrier gas (He) flow rate in the capillary column was 1.5 ml/min. The column temperature was initially held at 60°C for 1 minute, then ramped at 10°C/min up to 100°C, at 4 °C/min up to 190°C and finally at 6°C/min up to 310°C.

The product structures were assigned by MS spectra, the relative concentrations were quantified by ratio of the area of the respective FID (Flame Ionized Detector) peaks with respect to the total area. Emission spectra were collected by using a spectrograph Shamrock 303i (1200 gr/mm grating, 300nm blaze), and an intensified CCD (Andor DH334T-18U-03).

Theoretical Method

Stable and transition structures (TS), corresponding to minima and first order saddle points on the energy hypersurface, were determined by Density Functional Theory (DFT),[33] using the M06-2X functional[34] and gradient procedures[35]. The polarized split valence shell 6-311G(d,p)[36] was used in the DFT optimizations, and the nature of the critical points was checked by vibrational analysis. The energies were then refined by single-point energy computations with Dunning's (polarized, valence-3ζ) cc-pV*TZ* basis

set.[37] Hence the overall theory level is DFT(M06-2X)/cc-pV*TZ*//DFT(M06-2X)/6-311G(d,p). On the basis of previous studies[38,39] it is expected to perform acceptably. It is also apt to allow, in principle, the possible stacking of PAH-like parts of our growing systems, though stacking is expected to be of limited importance, due to the modest system size and flexibility.[40] Its performance in reactions involving radicals is also illustrated in the Supplementary Information, section 1.

For singlet diradicaloid structures, the wavefunction stability was checked, and obtained by relaxing it in the orbital rotations space. In any case, the desired spin densities, as expected for diradical structures, were obtained together with the wavefunction stability. The "automatic" closed shell singlet solution, obviously yields, instead, zero spin densities. Since the resultant spin-mixing gives a better description of the electron distribution but alters the energy, the energy values were refined by Yamaguchi's formula.[41]

The 6-311G(d,p) thermochemical corrections gave estimates of the zero point vibrational energy (ZPE), by which the cc-pV*TZ* relative energies were corrected [$\Delta E_{ZPE} = \Delta(E+\mathrm{ZPE})$]. Also the relative Gibbs free energies (ΔG) were estimated (within the usual approximations)[42] within a range of temperatures appropriate to encompass the sharply different conditions of the processes hinted to in the Introduction. Since the theoretical study focuses of course mainly on the experiment, ΔG at T = 400 K are reported in the Schemes. Given the experiment conditions, we can consider all species in thermal equilibrium with the surrounding gas. For this reason, we discuss in the text each $\Delta G^{\ddagger}$ barrier at 400 K with respect to the preceding minimum. When no TS on the *E* hypersurface is present, as in some radical couplings, and an all-downhill path to the intermediate product was found, the *G* surface was then probed, looking for a possible maximum. It was done by drawing *G* profiles along a path defined by series of constrained optimizations on the *E* surface, carried out at fixed values of a chosen distance R between the two moieties (see subsection B3). To define a G value, the vibrational frequency corresponding to the reaction coordinate was projected out.[43] The rate constants were estimated by using the Eyring equation within the Transition State Theory approximation.

Quantum mechanical calculations were carried out by using the GAUSSIAN09 system of programs.[44] Some kinetic tests were carried out by the numerical methods implemented in the program DYNAFIT.[45] Estimates to the rate constants were obtained by using Eyring's equation.

Results and Discussion

A. Experimental results.

The concentration values reported below refer to compounds that condensed in the cold trap. The main naphthalene impurities (measured without plasma) are: methyl-naphthalene isomers ($C_{11}H_{10}$) 410 ppm; dihydronaphthalene isomers $C_{10}H_{10}$ + tetrahydro-naphthalene $C_{10}H_{12}$ 180 ppm; naphthol isomers $C_{10}H_8O$ 130 ppm. This is consistent with the assay (99.9%) of the used naphthalene.

The main products, after the interaction of naphthalene with the post-discharge flow at position P1, are:

a) Initial O_2=0%, plasma power 14 W: dihydronaphthalene isomers $C_{10}H_{10}$ + tetra-hydronaphthalene $C_{10}H_{12}$ 2700 ppm; naphthol isomers $C_{10}H_8O$ 1100 ppm; methyl-naphthalene isomers $C_{11}H_{10}$ 280 ppm; binaphthalene isomers $C_{20}H_{14}$ 144 ppm.

b) Initial O_2 = 0.5%, plasma power 11 W: naphthol isomers $C_{10}H_8O$ 6430 ppm; dihydro-naphthalene isomers $C_{10}H_{10}$ + tetrahydronaphthalene $C_{10}H_{12}$ 730 ppm; naphthoquinone $C_{10}H_6O_2$ 670 ppm; dihydroepoxynaphthalene isomers $C_{10}H_8O$ 590 ppm; methylnaphtha-lene isomers $C_{11}H_{10}$ 360 ppm.

c) Initial O_2 = 4%, plasma power 1.4 W: naphthol isomers $C_{10}H_8O$ 4330 ppm; dihydroepoxynaphthalene isomers $C_{10}H_8O$ 600 ppm; naphthoquinone $C_{10}H_6O_2$ 470 ppm; methylnaphthalene isomers $C_{11}H_{10}$ 560 ppm.

In addition we detected non quantifiable traces of $C_{20}H_{14}O$, $C_{10}H_{10}O$, $C_{10}H_{12}O$, hydroxybenzaldehyde $C_7H_6O_2$, 2-formylbenzaldehyde $C_8H_6O_2$, and $C_{20}H_{14}O_2$.

Experimental results indicate that reactions of naphthalene with reactive oxygen species, at least within our experimental conditions, generate mainly oxygenated products (of slightly higher molecular weight), and give only a small contribution to a more substantial molecular growth.

B. Reaction pathways.

The focus of the theoretical-modelistic part of this study is on the possible routes to oxygenated products. Among them, we explored possible reaction pathways not only to the most important characterized products (naphthol, naphtho-1,4-quinone), but also to a minor but interesting product, which corresponds to a substantial mass increase. In fact, growth takes place via addition of a second naphthalene unit, and can consequently hint to the very early nucleation stages of oxidized carbon nanoparticles. Therefore, Scheme 1 (pathways which originate from the reactants, labeled **0**, to 1-naphthol **2**) and Scheme 2 (pathways to di-1-naphthylether **9**) describe evolutions of a reacting system composed by one or two naphthalene molecules, plus O (^{3}P), HO ($^2\Pi_{3/2}$), O_2 ($^3\Sigma_g^-$), and H. The reactions involving these species are considered in different sequences. Then, Scheme 3 shows how naphtho-1,4-quinone can form. The reactants' level, defined by the mentioned reactant species together, is the reference for the energetics reported in the Schemes as ΔG at T = 400 K (the experiment temperature). A few exceptions regarding the reference for ΔG differences have been introduced for sake of clarity, and explained in the legend of Scheme 2. Since an efficient thermalization can be safely assumed on the basis of the experiment conditions, we report instead in the text $\Delta G^{\ddagger}$ values with respect to each preceding minimum (barrier heights). Both hydroxyl and ground state oxygen atom are considered as very reactive species, capable of triggering some reaction sequence towards oxygenated stable products. In the Supplementary Information[46] Scheme S1 is also presented, to briefly comment on possible actions by ozone and the lowest singlet dioxygen state, and Scheme S2 reports some side steps departing from Scheme 1.

B1. Pathways to 1-naphthol at T = 400 K. HO and O can give radical addition to the aromatic π system. They can in principle also abstract a hydrogen from naphthalene (see point b below). Position 1 is chosen here to study both steps.

a. O and HO additions to naphthalene. Scheme 1 shows that from the reactants (**0**), upon O atom π–addition to naphthalene ($\Delta G^{\ddagger}$ = 10.2 kcal mol^{-1}) a first triplet adduct is obtained (**1**), which lies 12.7 kcal mol^{-1} below the reactants reference level. This $C_{10}H_8O$ species can undergo isomerization via 1,2 H shift to triplet naphthol (^{3}**2**). Though ^{3}**2** is located at -29.2 kcal mol^{-1}, the relevant barrier ($\Delta G^{\ddagger}$ = 26.1 kcal mol^{-1}) is quite high. Therefore, this first pathway does not seem to be promising for naphthol formation. An alternative step is H loss from **1**, to give the 1-naphthoxyl radical **3**. When dealing with H

losses, we report in Scheme 1 the energetics for the unimolecular homolytic H loss as black ΔG data. These provide a reference for H abstraction steps conducted instead by: O_2 ($^3\Sigma_g^-$), magenta figures; O (^{3}P), blue figures; or HO ($^2\Pi_{3/2}$), red figures (but possibly acquire also some importance in themselves at the highest T values). For the **1**–**3** step, the datum for O-mediated H abstraction is not present in Scheme 1, because O operates in this case differently: it adds to the oxyl oxygen and gives a peroxyl diradical (as discussed in the Supplementary Information,[46] Section 4). The most favorable pathway to obtain the intermediate **3** (irreversibly) is via H abstraction by HO, by overcoming a barrier of 6.3 kcal mol^{-1}. The intermediate **3** is a resonant species, with spin densities mainly on oxygen and on the two "allylic" position of the substituted ring (compare sketch). The spin density distribution obtained for **3** should actually favor those radical spin couplings with a H atom that involve its 2 and 4 positions.[47] A significant uncertainty about the assignment of the peak either to naphthol **2** or to its isomeric ketones inhibits assessing experimentally which channel (between going through **3** or through **4**) is more important. On the other hand, the relevant computed barriers for the steps departing from **3** are almost identical.

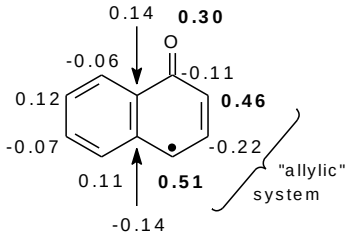

The HO radical addition to the π system of naphthalene (bottom of Scheme 1) presents a barrier close to that of the O atom addition ($\Delta G^{\ddagger}$ = 10.3 kcal mol^{-1}), and also the radical **4** so obtained is located close to **1**, at 12.4 kcal mol^{-1} below the reactants. So, **1** and **4** are expected to form with the same intrinsic rate and irreversibly. A theoretical estimate of their relative amounts would depend in the end upon hypothesized initial densities of O and HO. As before, different H loss modes can take place, of which H abstraction by O this time takes place (compare step **1**–**3**). Moreover, it is the easiest, since it presents a barrier of only 0.4 kcal mol^{-1}. HO comes next and requires overcoming a barrier of 4.5 kcal mol^{-1}. The final product, singlet 1-naphthol **2**, is again unavoidably associated with a multiplicity of ΔG values, depending on the nature of the preceding H loss.

Among the π–addition promoted pathways to ^{1}**2**, that by HO, followed by H abstraction by the O atom in **4**, which presents a very small barrier, would seem the most promising, on the basis of the free energy barriers only. On the same basis, however, **1** and **4** are formed as easily, and the two relevant backwards steps are not easy. Therefore, the computed kinetic constants describe **4**-**2** as a potentially more prompt naphthol production

channel, while **1**-**3**-**2** is expected to proceed more slowly –though inexorably– towards **3**, and then, with a barrier 7.3 kcal mol^{-1} high, irreversibly to its products. Therefore, a first point is that the relative *intrinsic* importance of the two pathways will be time-dependent.

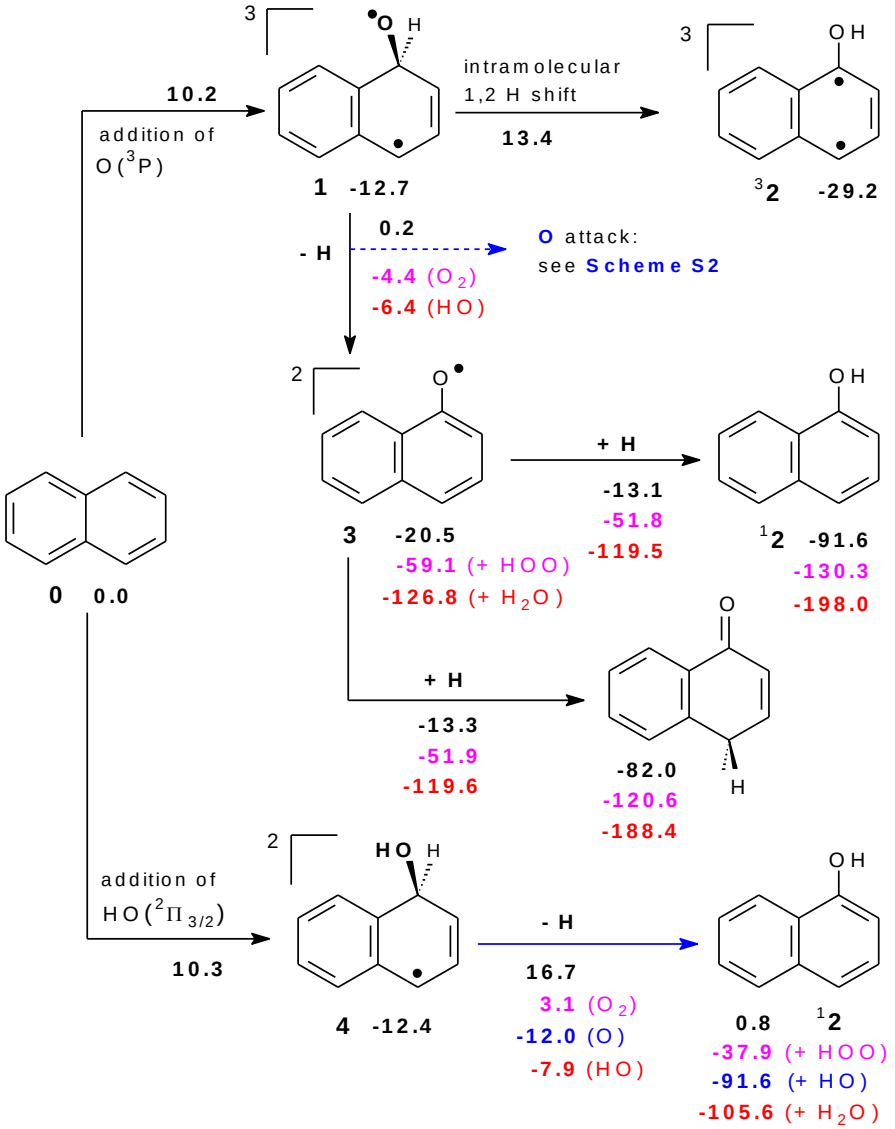

Scheme 1. Formation pathways for 1-naphthol ($C_{10}H_8O$). ΔG values at the DFT(M06-2X)/cc-pV*TZ*// DFT(M06-2X)/6-311G(d,p) computational level. Values originating from simple unimolecular homolytic H losses in black (taken as a reference); from bimolecular H abstractions operated by O_2 ($^3\Sigma_g^-$) in magenta, by O (^{3}P) in blue, and by HO ($^2\Pi_{3/2}$) in red.

A second important point is that their ability to produce naphthol will in the end depend on the concentrations of O and HO. Since an estimate of HO density is available from our measurements, while in our study a large uncertainty on O atom density subsists, we have carried out kinetic simulations,[45] within this simple scheme, hypothesizing three increasing O concentrations: 10^{12}, 10^{14}, and 10^{16} atoms cm^{-3} (the last one is that reported in refs. 29 and 30). Following this density sequence, the amount of naphthol produced via pathway **1**-

3-**2** varies from 35 to 65 and again 65% (where the step **1**-**3** proceeds via H abstraction by O_2, due to its higher concentration with respect to OH), and from 18 to 34 and 35% (step **1**-**3**: sheer H loss). Naphthol obtained through **4** has a role only at the lowest O density, since it drops from 47 to 1 and then to 0% (step **4**-**2**: H abstraction by O). More details are available in the Supplementary Information,[46] Section 6.

A possible intersystem crossing (ISC) in ^{3}**1** $\rightarrow$ "^{1}**1**" would give indeed a barrierless ring closure to the corresponding (closed shell) epoxide isomer. An epoxide product, and also another ether, a benzo-substituted 7-oxabicyclo [2.2.1]heptadiene, are in fact detected (see points b and c of subsection A).

b. Role of H abstraction from naphthalene. On the other hand, H abstraction from naphthalene (position 1 of naphthalene involved), if occurring, would imply the existence of an expectedly easy way to singlet 1-naphthol ^{1}**2**, via spin coupling between the hydroxyl and naphthyl radicals. (The naphthyl radical **5** will be further discussed below by making reference to Scheme 2, because it will also be invoked to interpret the formation of a minor product containing two naphthalene units.) The possible H abstraction from naphthalene operated by O or HO to give **5** has barriers, at T = 400 K, of 16.9 and 12.8 kcal mol^{-1}, respectively. Thus, addition at 400 K presents lower barriers than H abstraction, though this difference is only 2.5 kcal mol^{-1} in the case of HO intervention. These barriers translate to a kinetic datum, the branching ratio, for each species and for the two reaction types. The branching ratios are defined, for each process conducted by each reactive species X (O_2, O, HO), as $\alpha_X = k_X / \Sigma k_X$, where k_X is either the H loss rate constant from naphthalene, or an "effective" addition rate constant ($k_{add,eff}$) to naphthalene, for each X. The latter is defined by taking into account the two rate constants relevant to the addition step, k_1 and k_{-1}; then the role of the latter is damped by taking into account some possible exit channels from the adduct. See the Supplementary Information, section 2, for further details on the definition of the "effective" addition rate constant $k_{add,eff}$, and its behavior against the experimental data of Lorenz and Zellner for the reaction of hydroxyl and naphthalene.[48] Since we forcedly take into account only some of the exit channels, this damping provides only an upper limit of the influence of k_{-1}, which could actually be smaller if other exit channels were taken into account too. From another point of view, it provides a lower limit for the rate at which the reactant naphthalene disappears. In Σk_X, the summation runs over three "effective" additions and three H abstractions operated by X (see also the next

subsection for more details). The most prominent values at T = 400 K are, for the additions sketched in Scheme 1, α_O = 0.80, and α_{HO} = 0.18. The next values appear as minor contributions, which add up approximately to 2% of the total at the experiment temperature, and H-abstraction by HO does not seem capable of competing efficiently with the additions of the O atom or HO itself. In Scheme 1, to describe the most probable pathways towards 1-naphthol, contributing to the major isomer products, we have accordingly reported only the data for the most probable contributions.

The naphthyl radical **5** can form in principle in different ways: H abstraction by O_2, O, HO, and H. We find that their relative importance can vary drastically with temperature, and this aspect will be discussed in the next subsection B2. But another possibility for naphthyl formation could come from the exposure of naphthalene to UV radiation from de-excitation of present excited species, as HO, N_2, O, or He. We are however inclined to rule out this channel since their emission spectra have been recorded in the range 190-1000 nm, and the most energetic radiation available is one HO band at 280 nm. Since the threshold value for C–H homolysis is estimated to be 258 nm (from its D_e = 111 kcal mol^{-1}) we deem that discarding the contribution of a photolytic pathway is rather safe. A further point is that the presence of dioxygen is observed to quench significantly these emission bands.

B2. H-abstraction vs addition: T dependence. In the preceding subsection, when comparing the experimental results with the computational *G* barrier estimates at T = 400 K, H abstraction from naphthalene has been put aside as a potential minor contribution for naphthol formation. However, given the variety of situations envisaged in the Introduction, computational results for a range of temperatures up to 1300 K are also presented. In fact, an interesting point is inspecting if and how addition to the π–system of naphthalene can compete with hydrogen abstraction from it, when T is raised to combustion temperatures.

Figure 2 illustrates how the rate constants $k_{add,eff}$ (”effective”, for addition; continuous lines) and k_{abs} (H-abstraction from position 1; dashed lines) change with T. Two comparisons can be drawn. The first one is for each single species, HO or O (lines of the same color), comparing addition with H-abstraction. The second one between different species: the slopes of their lines will put their competition at each T on a ground that varies with T. For X = HO (red lines) not only the slopes but also the behavior of the $k_{add,eff}$ and k_{abs} lines are different. A crossing is present at ca. 850 K. For the oxygen atom, the two

blue lines start, at low T, more far apart; then they hint to a crossing at a higher T than HO, to be encountered at ca. 1600 K, as shown in the Supplementary Information, section 5. There, a more detailed comment on the changing slope of the HO addition line compared with the monotonic slope of its H abstraction counterpart can also be found.

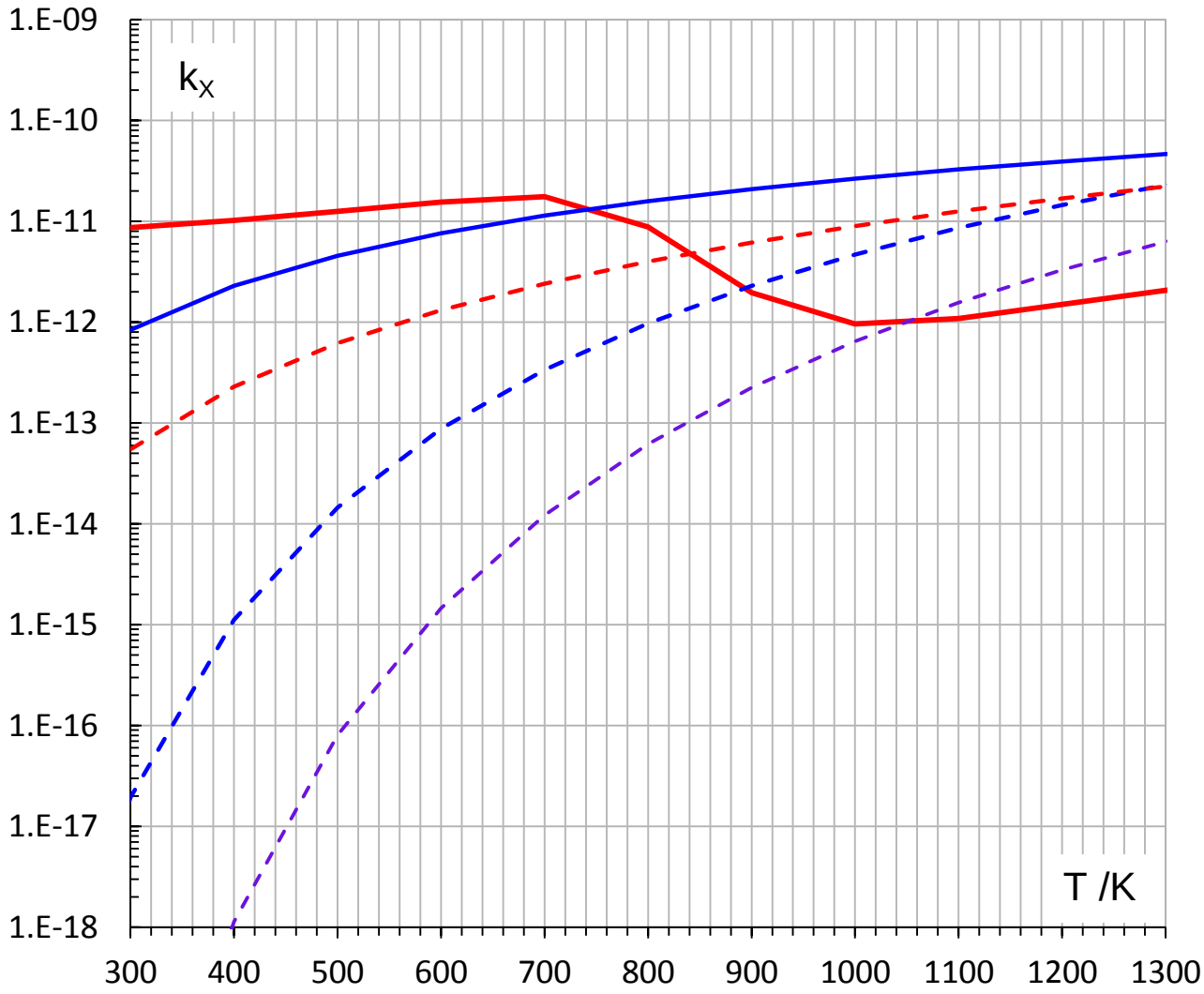

Figure 2. Rate constants k_X as a function of T. Red lines: X = HO; blue lines: X = O. k_X "effective" (see text) for X addition to naphthalene (continuous lines) vs H-abstraction from its position 1 (broken lines). For both species, addition is easier at lower temperatures; then, a crossing occurs for HO just around 850 K, and a similar crossing for O at ca. 1600 K (not represented here, see the ESI file, section 5).

Therefore, when both HO and O are present, addition dominates in the whole range 300–1300 K. It will be operated faster by HO up to ca. 750 K, then, beyond that temperature, the oxygen atom will add faster. On the other hand, H-abstractions by O and HO will tend to become as easy as HO addition around 850 K, where it declines, but are

still slower than O addition at the highest T values reported in Figure 2. Only at higher T values than represented (beyond 1600 K, approximately), the individual H abstractions will become faster.[49] HO is more inclined towards H abstraction than the oxygen atom up to ca. 1250 K, beyond the reverse is true.

A further piece of information is provided by the branching ratios $\alpha_X = k_X / \Sigma k_X$ (X=HO, O), whose values have already been briefly discussed in connection with the experiment temperature, 400 K. Since their variations with T reflect the behavior of a single kinetic constant k_X with respect to the sum of all five constants considered,[50] their growth and decline are very diverse, as can be seen in Figure 3. These are the data which, in conjunction with hopefully sensible guesses for the concentrations of the species discussed, at the various T values, might help us to interpret the outcome of the experiment in terms of product yields. Some density values are available in the literature for specific experiments, and extending over some temperature range,[17,21]

Generally, we see in Figure 3 that, at lower T values, additions (expressed as $\Sigma\alpha_X$, black continuous line) prevail, but decline constantly as T increases. By contrast, the $\Sigma\alpha_X$ for H abstractions (black dashed line) gradually becomes more important as T rises, with a crossing just beyond 1300 K (at lower T than suggested by the individual rate constants). Addition lines present conspicuous changes upon T variation. By contrast, H abstractions exhibit more moderate and monotonic changes, though slope variations are evident. Inspecting now each line in more detail, α_{HO} (addition) prevails completely at the lowest temperatures, but declines continuously, in steep way up to 900 K. By contrast, α_O (addition) rises as abruptly right from 300 K up to 900 K. Around 750 K it passes α_{HO}. Then, after a maximum at ca. 900 K, α_O keeps prevailing among additions up to ca. 1000 K, but it exhibits a regularly declining behavior.

The importance of H-abstraction from naphthalene (dashed lines) rises with T in a steeper way for the O atom (blue). These trends indicate qualitatively that the preferred pathways and the final outcome will depend significantly on temperature.

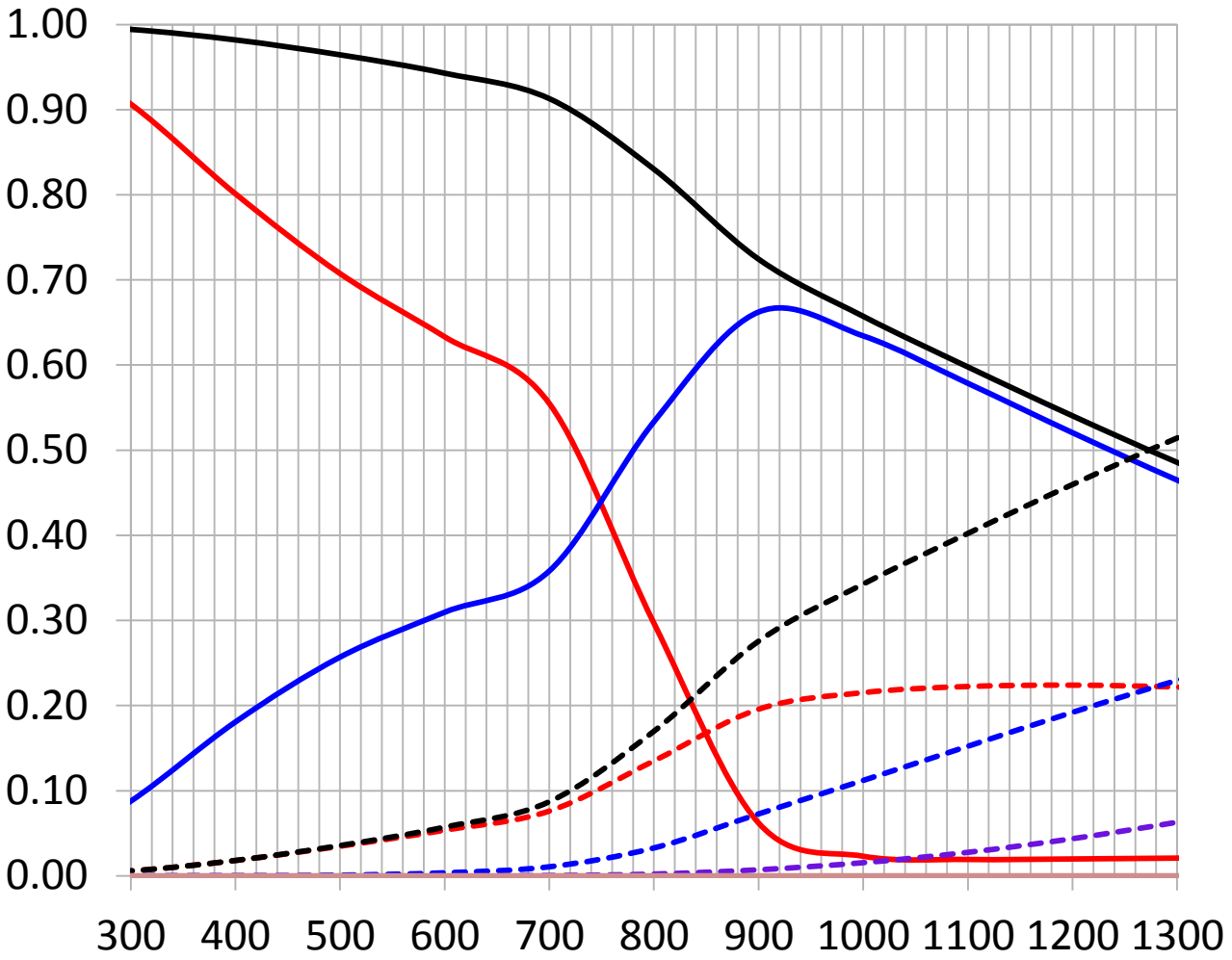

Figure 3. Branching ratios, defined for each reactive species X (X = HO, O, H) as $\alpha_X = k_X/\Sigma k_X$ (see main text). Addition to naphthalene: continuous lines. H-abstraction from its position 1: broken lines. Red lines: X = HO. Blue lines: X = O. Purple line: X=H. Black continuous line: sum of the two additions. Black dashed line: sum of the three H abstractions. At the lowest temperatures HO addition dominates, while O addition prevails beyond 800 K. Beyond 1300 K, H abstractions prevails.

B3. Mass increase pathways. Other bimolecular transformations of **1** or **3** involving again naphthalene might bring about an interesting growth of the initial reacting system through formation of oxygen-containing adducts (Scheme 2). It must be stressed that higher-mass products are detected at 400 K only in low concentrations. Radical addition of **1** to another naphthalene by engaging one of its "allylic" carbon (here explored only for position 4) is not promising since $\Delta G^{\ddagger}$ = 31.9 kcal mol^{-1}. It would produce the adduct **6** ($C_{20}H_{16}O$).

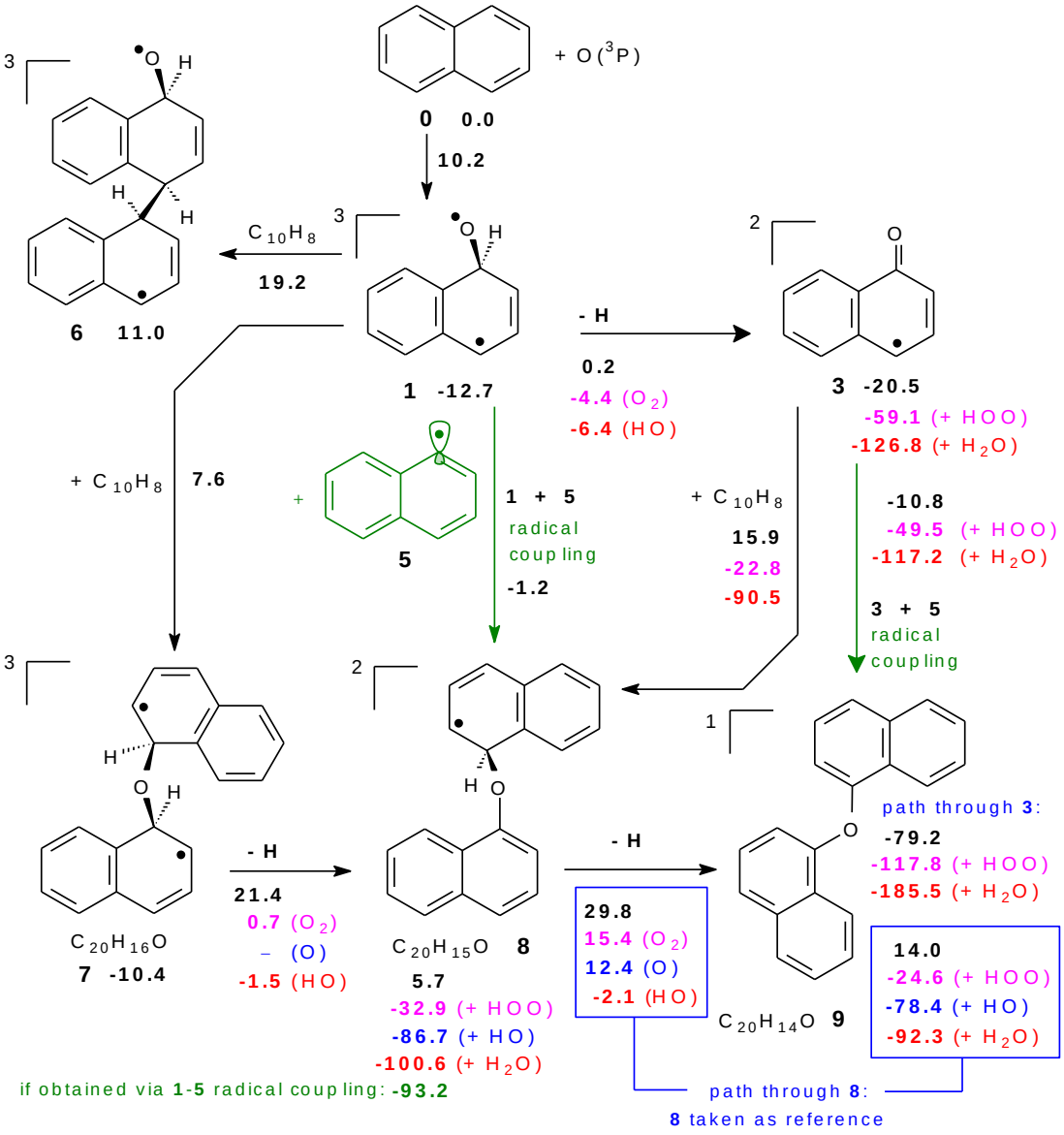

Scheme 2. Reactions of **1** and **3** with naphthalene which could cause a mass increase. ΔG values at the DFT(M06-2X)/cc-pVTZ//DFT(M06-2X)/6-311G(d,p) computational level. Values originating from unimolecular homolytic H losses in black; from H abstraction operated by O (^{3}P) in blue, by O_2 ($^3\Sigma_g^-$) in magenta and, by HO ($^2\Pi_{3/2}$) in red. Radical couplings are emphasized by the green color. Boxed values are taken with respect to **8**, to avoid reporting too many figures, which inevitably originate from "mixed steps" **7**-**8** and **8**-**9**. They allow a straightforward combination of values, as desired.

A better situation is encountered if the attack onto naphthalene is conducted by the oxyl terminal of **1**: it entails a barrier of 20.3 kcal mol^{-1}, to give the adduct **7**, located 10.4 kcal mol^{-1} below the reactants. Though the barrier is below the previous one, its height is not negligible. If **7** could be attained, then different H losses, from the position geminal to the oxyl oxygen, could follow to get **8** ($C_{20}H_{15}O$). The simple loss by homolytic bond cleavage, from which two fragments positioned 5.7 kcal mol^{-1} above the reactants are

obtained, requires overcoming a high barrier ($\Delta G^{\ddagger}$ = 31.8 kcal mol^{-1}) and is discarded again. If this step is instead mediated by O_2, the abstraction barrier is only 11.1 kcal mol^{-1} above **7**. For the O_2-mediated pathway, the products, **8** + HOO$^{\bullet}$, are placed 32.9 kcal mol^{-1} below the reactants. For the HO-mediated abstraction, the barrier is lower, 8.9 kcal mol^{-1} high with respect to **7**, and the attained well is even deeper: -100.6 kcal mol^{-1}, for **8** + H_2O. When the oxygen atom operates the H_{gem} abstraction from **7**, the resulting well is 86.7 kcal mol^{-1} deep, in correspondence of **8** + HO$^{\bullet}$. The step is apparently barrierless on the *E* hypersurface, but a *G* profile has not been defined because an alternative pathway, similarly ending to **8** formation, departs from **1** in a way significantly easier than the step **1**-**7**. Therefore, it is not worthwhile to insist in the laborious task of defining the *G* barrier for the O-mediated step **7**-**8**.

From **1**, the 1-naphthoxyl radical intermediate **3** forms via H loss. H loss can occur again by following steps of different nature (as already seen), with the exception of H abstraction by O (Scheme 3 below will illustrate the reaction of O with **3**). Then **3** can add to a naphthalene molecule and form **8**. The **3**–**8** addition step entails however a large barrier, because the intermediate **3** lies in more or less deep *G* wells: -20.5, -59.1, or -126.8 kcal mol^{-1}, respectively (HOO$^{\bullet}$ or HO$^{\bullet}$ or H_2O free energies taken into account). This trait makes the barrier for the step **3**–**8** 36.4 kcal mol^{-1} high, obviously in all three cases. The energetics reported for the intermediate **8** is the same, either if defined for the steps **1**-**7**-**8**, or from **1**-**3**-**8**, since in all cases the chemical events are the same, though taking place in a different order. In conclusion, since thermalization is assumed, both pathways examined so far, **1**-**7**-**8** and **1**-**3**-**8**, do not seem promising.

However, the intermediate **8** could be also obtained from the radical addition of **1** with the naphthyl radical **5**. In **1**, the spin density on C4 is 0.65 (0.56 on C2), while in **5** the unpaired electron is localized (spin density 1.03). This simple radical coupling does not present a barrier on the energy surface. Therefore, a maximum was defined along a free energy profile, by choosing, as intermoiety distance R, the C4(**1**)-C1(**5**) distance. The *G* maximum occurs early, in a geometrical sense, at R = 3.5 Å. The corresponding barrier is 11.6 kcal mol^{-1} high.

From **8**, however formed, and if formed, a further and final H loss would lead to **9** ($C_{20}H_{14}O$), which is detected experimentally in small amounts. Boxed free energy difference values are taken in this case with respect to **8**, departing from the choice of making

mostly reference, in the schemes, to the reactants level. This deviating choice is to avoid reporting a plethora of values, which unavoidably originate from the possibility of having "mixed" steps **7**-**8** and **8**-**9** (for instance, if first O_2 operates, then HO), plus from the radical coupling step. The boxed values allow a straightforward combination of values, as desired. The relevant $\Delta G^{\ddagger}$ barriers are: 29.8 kcal mol^{-1} for pure homolysis, but only 15.4 if the H abstraction is O_2-mediated, 12.4 if O-mediated, and even 2.1 kcal mol^{-1} below **8** if the abstraction is HO-mediated, due to the presence of a complex which precedes the TS.

Still another possibility is offered by the spin coupling between the radical **3** and naphthyl **5**. It stems from **3**, which forms in the easiest way, compared to **1**-**7** and **1**-**8**. Then the **3** + **5** addition requires overcoming a barrier of 9.6 kcal mol^{-1}. As seen before, the spin density on position 4 of **3** is 0.51, thus lower than the corresponding value in **1**, 0.65. This difference could explain why this radical coupling presents a barrier. To qualify these last channels, **1**-**8** and **1**-**3**-**8**, as more promising, we need first to pose the question of how much naphthyl **5** will be actually present. From the 1,1-binaphtyl detected, one could surmise that the naphthyl radical is present also at low temperatures, as that of the experiment.

***B4. A possible pathway to 1,4-naphthoquinone*.** Following initial O addition to naphthalene, a second barrierless O atom addition to intermediate **3** can take place. The intermediate **10** thus generated, is taken as a reference for the boxed free energy difference values of Scheme 3. When **10** undergoes H loss, **11** (1,4-naphthoquinone) is produced either by sheer homolysis (more demanding), or via H abstractions. The blue value (H abstraction conducted by an O atom) is again missing, as in Scheme 1 for the step **1**-**3**. It is not reported because, in **10**, the incoming O atom prefers again to add to the oxyl radical oxygen, rather than abstract its *gem* hydrogen.

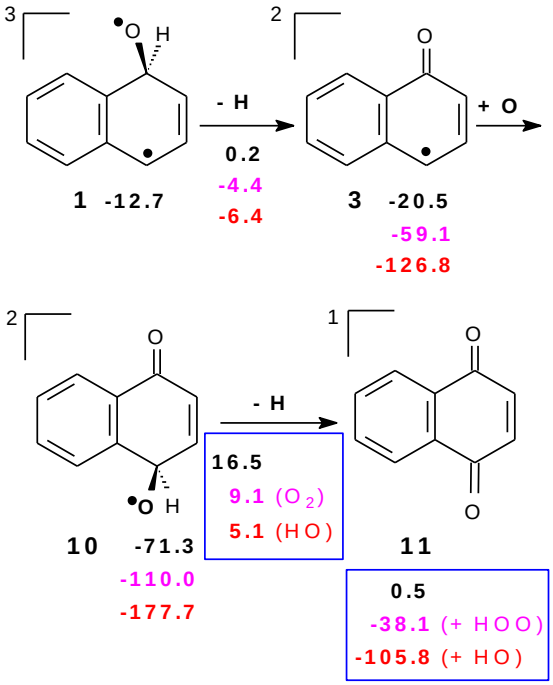

Scheme 3. Possible pathway to 1,4-naphthoquinone. Boxed values make reference to **10**.

Conclusions.

The reactions of naphthalene with oxygen species (O, OH, O_2) at 400 K produce mainly 1- and 2-naphtol, followed by 1,4-naphthoquinone, whose yield is one order of magnitude lower. Interestingly, also ether adducts with two naphthalene units form in smaller amounts. Thus oxidation reactions can promote the molecular growth of PAHs, in addition to producing oxygenated products.

Density functional calculations carried out to clarify the formation mechanisms, outline the critical role of HO, O and H additions to naphthalene, and H abstractions from it. At the experiment temperature (T = 400 K) addition reactions to naphthalene prevail, and explain the formation of naphthol. The dependence on temperature of these additions and of H abstraction processes suggests however that, upon temperature increase, the addition-initiated mechanism, described as dominant in the experiment, could be flanked by an abstraction-initiated one. Regarding the possible system growth by addition of a second naphthalene molecule, the most viable mechanism found relies on the presence of the naphthyl radical, and could consequently depend significantly on temperature. This suggests in turn a reason why at T = 400 K its yield is quite low: the H abstraction from

naphthalene is difficult. It is legitimate to surmise that, at a higher T, its yield might be larger.

Our results suggest that different oxidation/growth mechanisms prevail at different temperature. Thus there is no single pattern for PAH growth, which depends instead on the specific environment.

Acknowledgements. We acknowledge financial support from Provincia Autonoma di Trento and CNR-IMCB by the ENAM project. We also thank the staff of *Laboratori Didattici*, Department of Physics UNITN, who made available their instrumentation.

References and notes

1 A. D'Anna*, Proc. Comb. Inst.*, 2009, **32**, 593–613.

2 U. Pöschl, T. Letzel, C. Schauer,R. Niessner, *J. Phys. Chem. A*, 2001, **105**, 4029-4041.

3 R. M. Kamens, J. Guo, Z. Guo, S. R. McDow, *Atmos. Environ.*, 1990, **24A**, 1161-1173.

4 K.-H. Homann, *Angew. Chem. Int. Ed.,* 1998, **37**, 2434-2451.

5 (a) B. J. Finlayson-Pitts, J. N. Jr. Pitts, *Chemistry of the Upper and Lower Atmosphere*, Academic Press, New York, 2000, ch. 10. (b) See, in particular, Table 10.6.

6 See for instance: H. Böhm, H. Jander, *Phys. Chem. Chem. Phys.*, 1999, **1**, 3775-3781. E. B.Ledesma, M. A. Kalish, P. F. Nelson, M. J. Wornat, J. C. Mackie, *Fuel*, 2000, **79**, 1801-1814. I. Naydenova, P. A. Vlasov, J. Warnatz, *Proc. Eur. Comb. Meeting* 2005. C.Jäger, F. Huisken, H. Mutschke, I. Llamas-Jansa, Th. Henning, *Astrophys. J*., 2009, **696**, 706-712. C. Jäger, H. Mutschke, F. Huisken, S. Krasnokutski, A.Staicu, Th. Henning, W. Poppitz, I. Voicu, *Astrophys. J. Suppl*., 2006, **166**, 557-566.

7 L. A. Sgro, A. Simonelli, l. Pascarella, P. Minutolo, D. Guarnieri, N. Sannolo, P. Netti, A. D'Anna, *Environ. Sci. Technol*., 2009, **43**, 2608–2613.

8 Two recent reviews: A. G. G. M. Tielens, *Rev. Mod. Phys*., 2013, **85**, 1021-1081. M. Agúndez, V. Wakelam, *Chem. Rev*., 2013, **113**, 8710-8737.

9 S. E. Malek, J. Cami, J. Bernard-Salas, *Astrophys. J*., 2012, **744**, 16-24. C. Boersma,C. W. Jr. Bauschlicher, A. Ricca, A. L. Mattioda, E. Peeters, A.G. G. M. Tielens, L. J. Allamandola, *Astrophys. J.*, 2011, **729**, 64-78. J. M. Bakker, B. Redlich, A. F. G. van der Meer, J. Oomens, *Astrophys. J.*, 2011, **741**, 74-83. A.G.G.M. Tielens, *Ann. Rev. Astron. Astrophys*., 2008, **46**, 289-337. P. M. Woods, K. Willacy, *Astrophys. J*., 200, 7**655**, L49–L52. E. F. van Dishoeck, PNAS, 2006, **103**, 12249–12256. E. H. Wilson, S. K. Atreya, *Planet. Space Sci.*, 2003, **51**, 1017-1033. I. Cherchneff, J. R. Barker, A. G. G. M. Tielens, *Astrophys. J*., 1991, **377**, 541-552. L. J. Allamandola, A. G. G. M. Tielens, J. R. Barker, *Astrophys. J. Suppl. Series*, 1989, **71**, 733-775.

10 A. Occhiogrosso, S. Viti, N. Balucani, *MNRAS,* 2013, **432**, 3423–3430.

11 P. F. Goldsmith, R. Liseau, Tom A. Bell, John H. Black, J.-H. Chen, D. Hollenbach, Michael J. Kaufman, D. Li , D. C. Lis , G. Melnick, D. Neufeld, L. Pagani , R. Snell , A. O. Benz, E. Bergin , S. Bruderer , P. Caselli, E. Caux , P. Encrenaz, E. Falgarone, M. Gerin, J. R. Goicoechea , Å. Hjalmarson , B. Larsson, J. Le Bourlot, F. Le Petit , M. De Luca, Z. Nagy , E. Roueff , A. Sandqvist , F. van der Tak , E. F. van Dishoeck , C. Vastel , S. Viti , Umut Yıldız, *Astrophys. J.* 2011, **737**, 96-113. U. A. Yıldız, K. Acharyya, P. F. Goldsmith, E. F. van Dishoeck, G. Melnick, R. Snell, R. Liseau, J.-H. Chen, L. Pagani, E. Bergin, P. Caselli, E. Herbst, L. E. Kristensen, R. Visser, D. C. Lis, M. Gerin, *A&A*, 2013, **558**, A58.

12 J.F.Griffiths,J. A. Barnard, *Flame and Combustion*, Blackie Academic and Professional, 1995, § 6.8; in particular: pp 117 and 118. The crossings in Figure 6.7 are related to the bell-shaped soot yield curves, as a function of T, which are observed oftentimes (see ref. 20 Ch. 18, in particular pp 294 and 295).

13 H. S. Homan, *Comb. Sci. Tech*., 1983, **33**, 1-15.

14 N. E. Sánchez, A. Callejas, Á. Millera, R. Bilbao, M. U. Alzueta, *Energy & Fuels*, 2013, **27**, 7081-7088.

15 J. Xi, B.-J. Zhong, *Chem. Eng. Technol.*, 2006, **29**, 665-763.

16 B. R. Stanmore, J. F. Brilhac, P. Gilot, *Carbon*, **39**, 2001,2247-2268.

17 F.Xu, A. M. El-Leathy, C.H. Kim, G. M. Faeth, *Comb. Flame*, 2003, **132**, 43–57.

18 On soot gasification by O_3 and NO_2: S. Kamm, H. Saathoff, K.-H. Naumann, O. Möhler, U. Schurath, *Comb. Flame*, 2004, **138**, 353-361.

19 Two DFT studies modeling gasification: A. Montoya, F. Mondragòn, T. N. Truong Fuel *Proc. Tech*., **77–78**, 2002, 125-130. J. F. Espinal, A. Montoya, F. Mondragòn, T. N. Truong *J. Phys. Chem.* B, **108**, 2004, 1003-1008.

20 J. Warnatz, U. Maas, R. W. Dibble, *Combustion* 4th edition, Springer, Verlag, 2006, chapter 18, pp 282-296.

21 C.H. Kim, F. Xu, G. M. Faeth, *Comb. Flame*, 2008, **152**, 301–316.

22 I. Glassman, R. A. Yetter, *Combustion*, 4th edition, Elsevier, 2008, chapter 8.E, in particular §3.

23 S. Thomas, E. B. Ledesma, M. J. Wornat, *Fuel*, 2007, **86**, 2581–2595.

24 S. Thomas, M. J. Wornat, *Fuel*, 2008, **87**, 768–781.

25 A. Fuentes, R. Henríquez, F. Nmira, F. Liu, J.-L. Consalvi, *Comb. Flame*, 2013, **160**, 786–795.

26 D. Ascenzi, P. Franceschi, G. Guella, P. Tosi, *J. Phys. Chem.* A, 2006, **110**, 7841-7847.

27 A. A. Abdelaziz,T. Seto, M. Abdel-Salam, Y. Otani, *J. Hazard. Materials*, 2013, **246**, 26-33.

28 The similar “benzene plus O atom” reacting system has been the subject of theoretical (a-c), or joint experimental/theoretical (d), studies appeared in recent years. (a) J. F. Orrego, T. N. Truong, F. Mondragòn, *J. Phys. Chem.* A, 2008, **112**, 8205–8207. (b) T. L. Nguyen, J. Peeters, L. Vereecken, *J. Phys. Chem.* A, 2007, **111**, 3836-3849. (c) G. Vourliotakis, G. Skevis, M. A. Founti, *Energy Fuels*, 2011, **25**, 1950–1963. (d) C. A. Taatjes, D. L. Osborn, T. M. Selby, G. Meloni, A. J. Trevitt, E. Epifanovsky, A. Krylov, B. Sirjean, E. Dames, H. Wang, *J. Phys. Chem.* A, 2010, **114**,

3355–3370. S.J. Sibener, R.J. Buss, P. Casavecchia, T. Hirooka, Y. T. Lee, *J. Chem. Phys.*, 1980, **72**, 4341-4349 . H.-F. Chen, C.-W. Liang, J. J. Lin,Y.-P. Lee,J. F. Ogilvie, Z. F. Xu, M. C. Lin, *J. Chem. Phys.*, 2008, **129**, 174303

29 J. Y. Jeong, J. Park, I. Henins, S. E. Babayan, V. J. Tu, G. S. Selwyn, G. Ding, R. F. Hicks, *J. Phys. Chem.* A, 2000, **104**, 8027-8032.

30 S. Reuter, K. Niemi, V. Schulz-von der Gathen, H. F. Döbele, *Plasma Sources Sci. Technol.*, 2009, **18**, 015006.

31 G. Dilecce, L. M. Martini, M. Scotoni, P. Tosi, to be published.

32 S. Hofmann, A. F. H. van Gessel, T. Verreycken, P. Bruggeman, *Plasma Sources Sci. Technol.*, 2011, **20**, 065010.

33 R. G. Parr, W. Yang, *Density Functional Theory of Atoms and Molecules,* Oxford University Press, New York, 1989, ch. 3.

34 Y. Zhao, D. G. Truhlar, *Theor. Chem. Acc.*, 2008, **120**, 215-41.

35 J. A. Pople, P. M. W. Gill, B. G. Johnson, *Chem. Phys. Lett.*, 1992, **199**, 557-560. H. B. Schlegel, *Computational Theoretical Organic Chemistry,* ed. I. G. Csizsmadia, R. Daudel, Reidel Publishing Co., Dordrecht, The Netherlands, 1981, pp. 129-159. H. B. Schlegel, *J. Chem. Phys.*, 1982, **77**, 3676-3681. H. B Schlegel, J. S. Binkley, J. A.; Pople, *J. Chem. Phys.*, 1984, **80**, 1976-1981. H. B. Schlegel, *J. Comput. Chem.*, 1982, **3**, 214-218.

36 R.Krishnan, J. S. Binkley, R. Seeger, J. A. Pople, *J. Chem. Phys.*, 1980, **72**, 650-654.

37 R. A. Kendall, T. H., Jr. Dunning, R. J. Harrison, *J. Chem. Phys.*, 1992, **96**, 6796-806.

38 D. Trogolo, A. Maranzana, G. Ghigo, G. Tonachini, *J. Phys. Chem.* A 2014, **118**, 427−440.

39 Y. Zhao , D. G. Truhlar, *Acc. Chem. Res.*, 2008, **41**,157-167.

40 A. Maranzana, A. Indarto, A. Giordana, G. Tonachini, V. Barone, M. Causà, M. Pavone, *J. Chem. Phys.*, 2013, **139**, 244306.

41 S. Yamanaka, T. Kawakami, K. Nagao, K. Yamaguchi, *Chem. Phys. Lett.*, 1994, **231**, 25-33. K. Yamaguchi, F. Jensen, A. Dorigo, K. N. Houk, *Chem. Phys. Lett.*, 1988, **149**, 537-542. See also: J. Baker, A. Scheiner, J. Andzelm, *Chem. Phys. Lett.*, 1993, **216**, 380-388. For discussions concerning the effect of spin projection on the performances of DFT methods, see:. J. M. Wittbrodt, H. B. Schlegel, *J. Chem. Phys.*, 1996, **105**, 6574-6577; E. Goldstein, B. Beno, K. N. Houk, *J. Am. Chem. Soc.*, 1996, **118**, 6036-6043.

42 See for instance: W. J. Hehre, L. Radom, P. v. R. Schleyer, J. A. Pople, *Ab Initio Molecular Orbital Theory*, J. Wiley & Sons, 1985, Chapter 6.3. And, from the Gaussian site: http://www.gaussian.com/g_whitepap/vib.htm (on how vibrational frequencies are computed) and http://www.gaussian.com/g_whitepap/thermo.htm (on the computation of partition functions and Gibbs free energy).

43 A.G. Baboul, H. B. Schlegel, *J. Chem. Phys.*, 1997, **107**, 9413-9417.

44 Gaussian 09, Revision A.02, M. J. Frisch, G. W. Trucks, H. B. Schlegel, G. E. Scuseria, M. A. Robb, J. R. Cheeseman, G. Scalmani, V. Barone, B. Mennucci, G. A. Petersson, H. Nakatsuji, M. Caricato, X. Li, H. P. Hratchian, A. F. Izmaylov, J. Bloino, G. Zheng, J. L. Sonnenberg, M. Hada, M.

Ehara, K. Toyota, R. Fukuda, J. Hasegawa, M. Ishida, T. Nakajima, Y. Honda, O. Kitao, H. Nakai, T. Vreven, J. A. Montgomery, Jr., J. E. Peralta, F. Ogliaro, M. Bearpark, J. J. Heyd, E. Brothers, K. N. Kudin, V. N. Staroverov, R. Kobayashi, J. Normand, K. Raghavachari, A. Rendell, J. C. Burant, S. S. Iyengar, J. Tomasi, M. Cossi, N. Rega, J. M. Millam, M. Klene, J. E. Knox, J. B. Cross, V. Bakken, C. Adamo, J. Jaramillo, R. Gomperts, R. E. Stratmann, O. Yazyev, A. J. Austin, R. Cammi, C. Pomelli, J. W. Ochterski, R. L. Martin, K. Morokuma, V. G. Zakrzewski, G. A. Voth, P. Salvador, J. J. Dannenberg, S. Dapprich, A. D. Daniels, Ö. Farkas, J. B. Foresman, J. V. Ortiz, J. Cioslowski, and D. J. Fox, Gaussian, Inc., Wallingford CT, 2009.

45 P. Kuzmič, *Anal. Biochem.*, 1996, **237**, 260-273. (http://www.biokin.com/dynafit/index.html). See also: P. Kuzmič, DynaFit, Version 4.0, May 2014**.**

46 Electronic Supplementary Information (ESI) available: [validation of the computational level, schemes with possible roles of O ($^1\Delta_g$), O_3, hydroperoxide, comparison with experimental data, kinetic simulations, Table of energies, and optimized geometries]. See DOI: 0.1039/b000000x/.

47 A side result is that the H addition to position 4 is described computationally as giving a ketone which is located 9.7 kcal mol^{-1} higher in energy than ^{1}**2**.

48 (a) R. Atkinson *J Phys Chem Ref Data*, Monograph 1, 1989; in particular, for naphthalene, see page 237. (b) K. Lorenz, L. Zellner *Ber. Bunsenges. Phys. Chem.* 1983, **87**, 629-636.

49 This is a behavior experimentally known also for other systems, as in the reaction of HO with alkylated benzenes. For toluene and 1,2,3-trimethylbenzene, an Arrhenius plot presents two distinct regions, with opposite slope, pertaining to addition and H-abstraction, and a transition zone, a discontinuity, located roughly around 340 K. See: R. A. Perry, R. Atkinson, J. N. Pitts jr, *J. Phys. Chem.*, 1977, **81**, 296-303. See also ref.48a, in particular pages 204-241. However, in our case, and for every abstracting species X, H-abstraction occurs at a higher temperature than in the alkylated benzenes case. This feature originates from the fact that aromatic hydrogens are much less inclined toward homolytic cleavage than those of alkyl groups bound to an aromatic ring. This trait is illustrated for instance by D_0 values: e.g. 111 kcal mol^{-1} to get the phenyl radical $Ph^{\bullet}$ from benzene, vs only 88 to get the resonance stabilized benzyl, $PhCH_2^{\bullet}$ from toluene. See: M. B. Smith, J. March, *March's Advanced Organic Chemistry*, 6th, Wiley-Interscience, 2007, Ch. 5, Table 5.4. R. H. Chen, S. A. Kafafi, S. E. Stein, *J. Am. Chem. Soc.*, 1989, **111**, 1418-1423.

50 H abstractions by HO, O, and H are taken into account. Concerning addition, only for HO and O addition are instead considered, because H addition to naphthalene, followed by H abstraction (from the saturated carbon) gives again naphthalene.